## EXECUTIVE SUMMARY:

This report documents the design, analysis, and testing of a small-scale wind turbine blade optimized for maximum torque output at Reynolds numbers between 9,300 and 21,000. The three-bladed rotor uses the S1223 airfoil, selected for its CL_max of 1.8-2.0 at Re ≈ 15,000, operating at tip-speed ratio λ = 3 and target rotational speed of 900 rpm. Design constraints included 6-inch maximum radius, 2-inch maximum chord, 2000 rpm speed limit, and Accura 25 SLA material with 38 MPa tensile strength.

The design process combined blade element momentum theory, ANSYS Fluent CFD simulation, and experimental validation. Blade geometry featured linear chord taper from 2.0 inches at root to 0.4 inches at tip, with twist ranging from 60° to 14° to maintain α ≈ 3° across the span. CFD predicted 11.03 W power output at design conditions. Structural analysis calculated failure wind speed of 67.73 m/s, providing a 10× safety margin over the 2.8-6.2 m/s operating range.

Despite some issues, physical testing revealed that maximum power output consistently occurred around 1300 rpm rather than the designed 900 rpm. Progressive loading from 2-10 volts on the magnetic brake prevented premature stall and enabled performance characterization across the torque range. Testing was limited by maximum allowable wind speed and brake capacity; as wind speed increased, the blade required progressively higher brake torque before stalling, indicating that maximum performance was not reached within test constraints. At 7 m/s and maximum brake loading, the blade operated at only 1300 rpm, well below the 2000 rpm safety limit, suggesting significant untapped performance potential at higher wind speeds. CAD-to-CFD workflow challenges required manual airfoil file editing and multi-segment lofting, introducing minor geometric deviations, however these changes were deemed negligible in regards to the results. Print quality issues and mounting errors affected initial testing but were resolved.

The design successfully demonstrated torque-optimized operation while satisfying all safety constraints. The 900-to-1300 rpm discrepancy and inability to reach maximum performance suggest the blade's aerodynamic capability exceeded both design predictions and available test conditions. Future iterations should optimize for higher operational speeds based on observed performance, expand testing to higher wind speeds to characterize true maximum output, improve CFD mesh quality to better predict high-performance regimes, and eliminate CAD export errors to ensure geometric fidelity.

## CONTEXT, OBJECTIVES, AND CONSTRAINTS

### Design Context:

This design operates in the Big Blue wind tunnel under a Weibull distribution (k=5, c=5 m/s), producing a mean wind speed of 4.6 m/s with a 90% confidence band from 2.8-6.2 m/s. Using the 2-inch maximum chord and air kinematic viscosity $v = 1.5\times10^{-5}$ m²/s, the Reynolds number ranges from 9,300 to 21,000 with a design point of Re = 15,550. Conventional NACA airfoils perform poorly in this regime because at low Reynolds numbers the boundary layer remains

laminar over most of the airfoil surface and cannot withstand adverse pressure gradients, leading to premature separation, reduced lift generation, and increased pressure drag, which led us to investigate specialized low-Re airfoils as discussed later. SLA printing in Accura 25 imposed additional constraints on minimum feature sizes, trailing edge thickness, and structural capacity.

**Technical Objectives:**

The primary objective was maximizing torque output across the wind distribution. This design prioritized high starting torque and low-speed operation. Selecting $\lambda = 3$ produces larger angles of attack (6-10° at mid-span) where the lift vector rotates significantly from the axial direction, creating strong tangential force components that drive rotation. This torque-focused approach accepts lower aerodynamic efficiency in exchange for reliable startup and stable operation in variable wind conditions. The target speed of 900 rpm was calculated from $\Omega = \lambda U/R = 3(4.59)/0.152 = 94.25$ rad/s, providing margin below the 2000 rpm safety limit.

**Design Constraints:**

Geometric: Maximum radius 6 inches (0.152 m), hub radius 1 inch (0.0254 m), maximum chord 2 inches (0.0508 m). These limits determined the aspect ratio and twist distribution.
Operational: Rotational speed limited to 2000 rpm for structural safety. The magnetic brake had a torque limit of 0.035 N·m, with the design ideally targeted to remain within this range for testing purposes. The design needed to operate across the full Weibull distribution while maintaining $\lambda = 3$.
Material: Accura 25 has a tensile strength of 38 MPa and flexural modulus of 1.6 GPa. Printing required minimum trailing edge thickness of 1.0 mm and root wall thickness of 2.0 mm. These material properties dictated section sizing and root reinforcement.
Aerodynamic: The Reynolds range of 9,300-21,000 required specialized low-Re airfoils with gentle stall behavior and high camber. These constraints were interconnected, requiring iterative design refinement to maximize torque while satisfying all requirements simultaneously.

**DESIGN PROCESS AND RATIONALE**

**Operating Point Establishment:**

Weibull analysis using the probability density function $p(U) = (k/c)(U/c)^{(k-1)}\exp(-(U/c)^k)$, where $k=5$ is the shape parameter and $c=5$ m/s is the scale parameter, yielded mean wind speed 4.59 m/s with 5th and 95th percentiles at 2.76 and 6.23 m/s. For the maximum allowable chord $c = 0.0508$ m (2 inches), Reynolds number $Re = Uc/v$, where $U$ is wind speed and $v = 1.5\times10^{-5}$ m²/s is air kinematic viscosity, spans 9,349-21,088 with $Re_{mean} = 15,548$, confirming a low-Re regime where laminar effects dominate. MATLAB scripts calculated these parameters to guide airfoil selection and performance prediction.

**Tip-Speed Ratio Selection and Torque Optimization:**

Tip-speed ratio fundamentally determines the torque-efficiency balance. This design prioritized high torque generation, as we ended up exceeding the magnetic brake's torque capacity for force needed to stall our blades during testing as described later. At high λ (> 6), blades move faster than the wind, creating small angles of attack and aligned lift vectors that produce high efficiency but low torque. At low λ (≈ 2-3), slower blade motion generates larger angles where lift contributes more tangentially to rotational moment. Selection of λ = 3 maintains an effective angle of attack at 6-10° where low-Re airfoils achieve maximum lift-to-drag ratio while rotating the lift vector substantially from the axial direction for strong tangential force. From λ = 3, U = 4.59 m/s, and R = 0.152 m, the target speed Ω = λU/R = 94.25 rad/s ≈ 900 rpm provides margin below the 2000 rpm safety limit.

**Airfoil Selection- S1223 Justification:**

Evaluation of NACA 4412 and S1223 using XFOIL and published wind tunnel data at Re ≈ 15,000 identified S1223 as optimal. As shown in the lift curve comparison (Figure 1), the S1223 achieves CL_max = 1.8-2.0 at Re = 10,000-20,000, nearly double that of NACA 4412. The S1223 maintains CL > 1.5 from 6-12° angle of attack while NACA 4412 peaks at CL ≈ 1.0. This exceptional lift generation translates directly to higher torque per unit span when projected tangentially through the inflow angle.
Second, the S1223 exhibits gentle stall behavior with gradual separation and maintained lift over a broad angle range, ensuring consistent torque during startup and operation outside the design range. Third, as shown in the aerodynamic efficiency comparison (Figure 2), the S1223 achieves peak lift-to-drag ratios of 50-60 near α = 3-5°, aligning with blade element theory predictions at λ = 3. The S1223 maintains superior L/D over NACA 4412 from 4-10°, precisely our anticipated operating range.
Fourth, the S1223's geometry provides practical advantages: 12% thickness supplies structural depth at the root while 8-9% camber maintains high-lift characteristics outboard. The pressure distribution on the S1223 helps prevent flow separation at low Reynolds numbers, critical for maintaining performance in our operating regime. The S1223's established use in model aircraft propellers and small wind turbines at Re < 100,000 provided additional confidence in its performance.

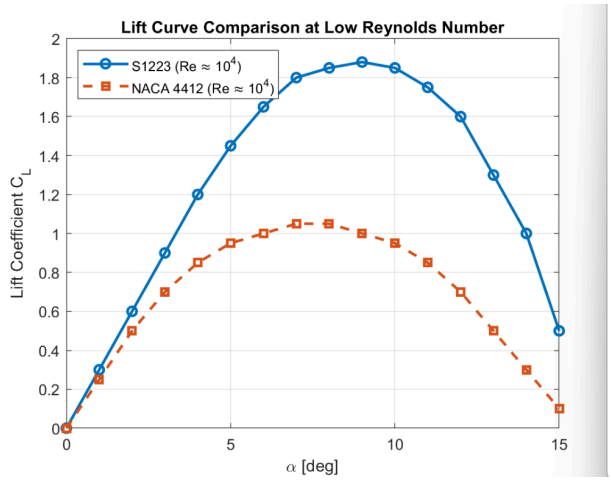


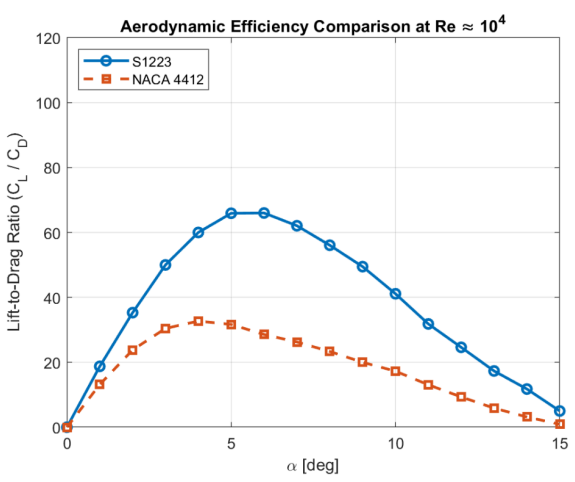

Figure 1: Lift Coefficient vs. AOA at Low Re  Figure 2: Lift-to-Drag Ratio vs. AOA at Re=$10^4$

Figure 1: Lift coefficient (left) Figure 2: Aerodynamic efficiency (right) comparison for S1223 and NACA 4412 airfoils at Re ≈ $10^4$, demonstrating S1223's superior performance in the low Reynolds number regime.

**Blade Geometry- Twist, Taper, and Pitch Distribution:**

Blade element momentum theory determined the twist distribution. The local inflow angle φ(r) = arctan(U/(Ωr)) was calculated assuming negligible induction. To maintain the optimal angle of attack α_opt ≈ 3° from S1223 data, the geometric pitch was set as β(r) = φ(r) - α_opt. This produced the following twist distribution: β ≈ 55-60° at r/R = 0.25 (root), β ≈ 36° at r/R = 0.40, β ≈ 30° at r/R = 0.50 (mid-span), β ≈ 21° at r/R = 0.70, and β ≈ 16° at r/R = 0.90 (near tip). The extreme root twist angles (r < 0.22R) were then attached to the cylindrical hub attachment at the thickest portion of the airfoil. This allowed for the greatest cross-section area between the airfoil and mounting geometry which improved printability and structural robustness with minimal loss of aerodynamic performance.
The chord distribution used a linear taper from 2.0 inches at the root to 0.4 inches at the tip. This taper maintains higher solidity inboard where tangential velocities are lower, reduces root bending moment by decreasing loads at outboard stations, and provides a structurally sound planform. The resulting aspect ratio of approximately 4.0 (R/c_mean = 6/1.5) balanced aerodynamic efficiency, structural stiffness, and manufacturing feasibility.

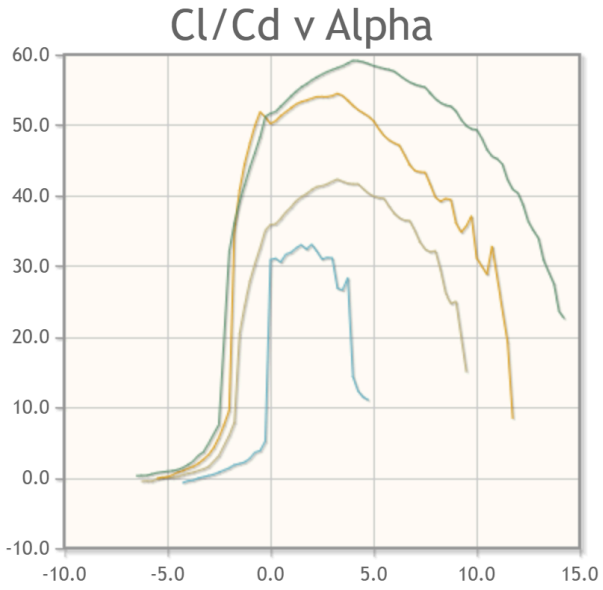


Figure 3: Cl/Cd vs. AOA

Figure 3 displays the S1223 aerodynamic efficiency (CL/CD) as a function of angle of attack across Reynolds number range. Peak efficiency occurs at α ≈ 3-5° for all Reynolds numbers, validating the selected design angle of attack of 3°.

**Structural Validation and Safety Analysis:**

MATLAB scripts computed bending moments along the blade span from distributed aerodynamic loads predicted by blade element theory. Each blade cross-section was modeled as a solid rectangle with thickness t = 0.12c, yielding section modulus $Z = bc^2/6$ where b is the chord. At the design point (U = 4.59 m/s), the maximum root bending moment was calculated as 0.022 N·m, below both the magnetic brake limit (0.035 N·m) and the material capacity.
To determine the structural failure wind speed, load scaling analysis was applied: since aerodynamic forces scale approximately with $U^2$ at constant λ, the critical wind speed is $U_{crit} = U\sqrt{(\sigma_{allow}/\sigma_{current})}$, where $\sigma_{allow}$ is the allowable stress and $\sigma_{current}$ is the current stress. Using Accura 25's tensile strength of 38 MPa, the analysis predicted structural failure at 67.73 m/s—more than 10× above the operating range of 2.8-6.2 m/s. Mid-span stress checks at r = 0.50R showed similar safety factors. A parametric sweep from 2-15 m/s confirmed that both torque and stress remained within acceptable bounds across the entire operating envelope.

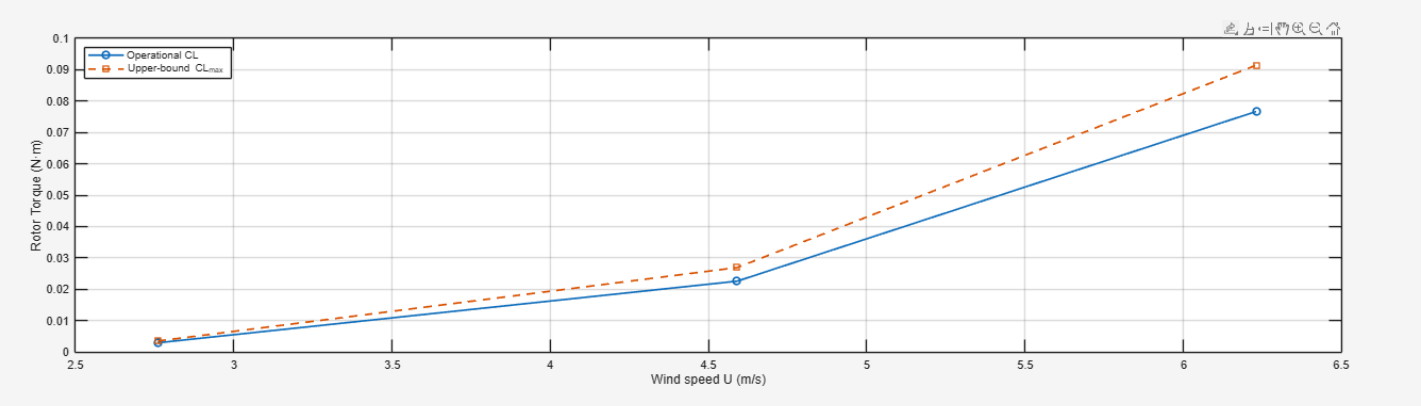


Figure 4: Rotor Torque [Nm] vs. Wind Speed [m/s]

Figure 4 displays the blade element momentum prediction of rotor torque across the wind speed range. Operational estimate uses CL = 1.1; upper bound uses CL_max = 1.3. At design point (U = 4.59 m/s), the predicted torque of 0.022 N·m remains within the brake capacity. Unfortunately, our blade outperformed our expectations in terms of lift coefficient, and as seen above, at higher wind speeds, we surpassed the torque brake upper limit of .035.

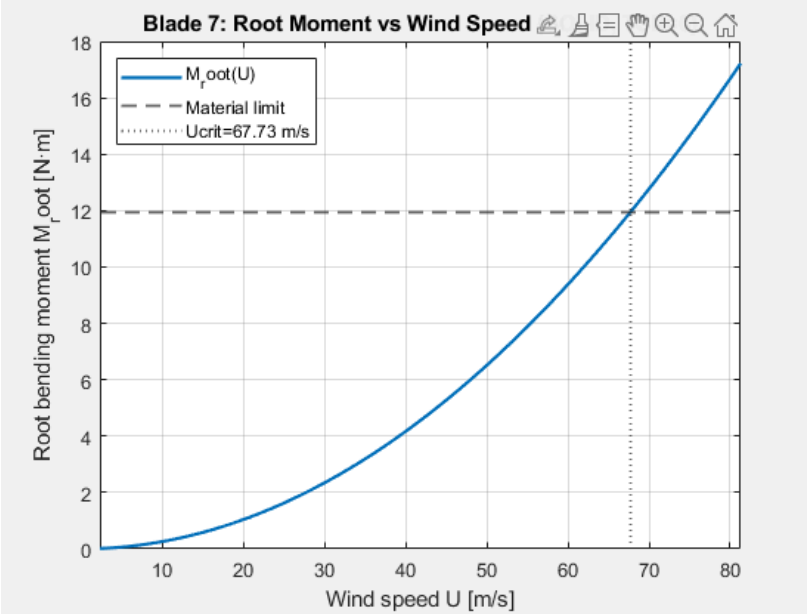

Figure 5: Root Bending Moment [Nm] vs. Wind Speed [m/s]

Figure 5 depicts the root bending moment as a function of wind speed with material limit shown. Critical failure wind speed of 67.73 m/s (U_crit) exceeds all expected operating conditions, confirming structural adequacy of the Accura 25 blade design.

**Operating Assumptions and Hypotheses:**

The design assumed that a low tip-speed ratio (λ ≈ 3) would produce higher torque than high-λ operation despite lower efficiency. At low λ, large angles of attack rotate the lift vector from the axial direction, creating strong tangential force components that drive rotation. Additionally, in the low-Re regime, the achievable power coefficient is inherently limited by laminar separation, meaning the efficiency penalty of choosing low-λ operation is less severe than it would be at higher Reynolds numbers.

Mean wind speed (4.59 m/s, Re ≈ 15,500) served as the primary design point, with performance verified across the 5-95% wind distribution. The design prioritized startup torque and steady low-speed operation over peak power coefficient, reflecting the practical requirement for reliable starting and stable operation under varying conditions.

Airfoil performance data from XFOIL and published sources at Re = 15,000-50,000 were used to approximate behavior in the Re = 9,000-21,000 range, justified by the S1223's documented performance in this regime. SLA printing was assumed to produce sufficiently smooth surfaces to approximate theoretical airfoil performance. Design required minimum trailing edge thickness of 1 mm and root wall thickness of 2 mm while accepting the inherent surface roughness of the printing process.

**Description of the approach followed to assess the actual performance of the design:**

To assess our design, we both used physical testing as well as CFD testing. Our physical testing model followed a modified procedure than the one outlined in our second deliverable. The initial procedure focused on finding various combinations of torque brake and wind speed combinations to maintain a 900 RPM angular velocity; however was corrected by staff to be an inefficient data collection procedure, and on the day of lab testing, had to come up with a new procedure. The new procedure, as mentioned above, was designed to capture and record the power able to be produced by our blade at each wind speed. The results of this procedure ideally would have allowed us to generate power curves for our blade that should have provided us insight into what RPM our maximum power generation occurred at throughout various wind speeds.

**Results: including whether or not your design achieved your initial objectives, whether or not all constraints were satisfied, any issues or challenges you faced throughout the process, and some reflection about your process: what went well, what was unexpected, and how you would approach a second iteration to improve your design further.**

Unfortunately, the day of testing had a few mishaps. Primarily, after figuring out our new testing procedure with limited insight from the advising TA, we soon discovered our data collection button within the VI was not working properly. As this was one of the last slots before Thanksgiving break, and the TA was unsure of how to fix it, advised us to take the data we deemed necessary. This combination of unfortunate events led us to an oversight in which we did not collect the RPM data for all of our trials and were only able to derive some RPM data from screenshots and memory. That said, our results were less than conclusive on the effectiveness of our design for optimizing power at 900 RPM, as we could not generate RPM power curves from our limited data. Obviously, if we were to redo the lab or experiment, it would be our top priority to ascertain that data point as well as collect power and wind speed. Data collection and analysis aside, it is important to note that our blade performed quite well in the wind tunnel simulation. We had no issues with startup even at low speeds, and our method of progressively increasing the torque gave us exceptional power output at the top end (~1 W). Our blade design, in some sense, was too strong for the current setup up as for our higher wind speeds, we were almost easily able to max out the torque brake. This was initially thought to be ok, as we designed assuming losses and inefficiency elsewhere in the blade.  Something to consider if we are to keep the same geometry would be to test again with a stronger torque brake, allowing us to capture a fuller range of values for our blade. Another option, keeping the same setup up would be to scale down our blade, keeping the same geometric proportions, so that the maximum force the blades could capture would be lower. So, to recap, our design outperformed our initial objectives, surpassing the upper limits set by the model. We had a few technical issues throughout our data collection process, but we identified clearly where we would revise our process and our design to maximize our power generation within the constraints of the testing apparatus.

**Solidworks Modeling:**

For both manufacturing and simulations, we needed a 3D model of our airfoil. To achieve this, we utilized SolidWorks to create the CAD model shown below in Figure 1. The airfoil is generated using a loft between several airfoil cross sections going down the span of the blade. Notably, the initial file submitted for 3D printing contained incorrect geometry on the mounting geometry. This mistake was caught early, and a second set of wings was printed for our wind tunnel testing. Another issue with the initial CAD design was that the trailing edge ended at a finite point.  This resulted in an unclosed STEP file, which became problematic for manufacturing and analysis.

When we received the blades from printing, they contained some missing chunks out of the trailing edge, as seen in Figure 2. The TAs speculated this was in part due to the unclosed STL file. Additionally, when we attempted to perform CFD analysis, we found it would be unsolvable without a closed STEP file. To remedy this issue, the data file, which contains the curve data for the airfoil, was edited to remove the finite point at the trailing edge. To close the airfoil, a curved arc bridged the gap at the trailing edge. However, with this modification, the loft was unsolvable. Thus, instead of making a continuous loft throughout each section, individual lofts between adjacent sections were merged together. This resulted in sharp edges between the lofts as seen in Figure 3. However, the overall geometry largely matches our design, so it was deemed acceptable for CFD analysis.

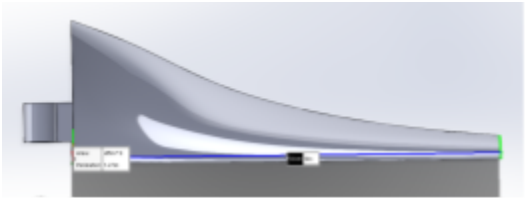

Overall Dimensions

Twist

Figure 6: Overview of CAD model

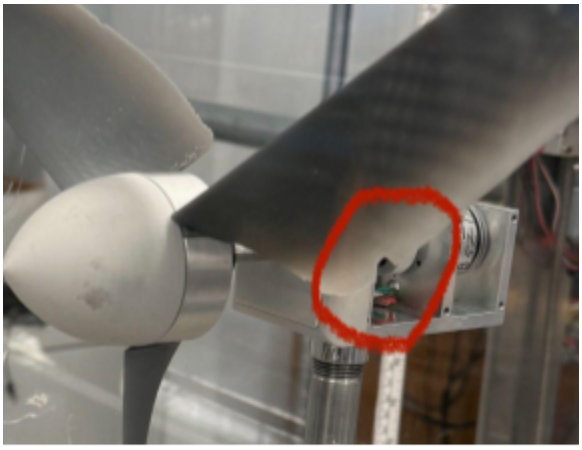

Figure 7: Printing errors in airfoil (circled in red)

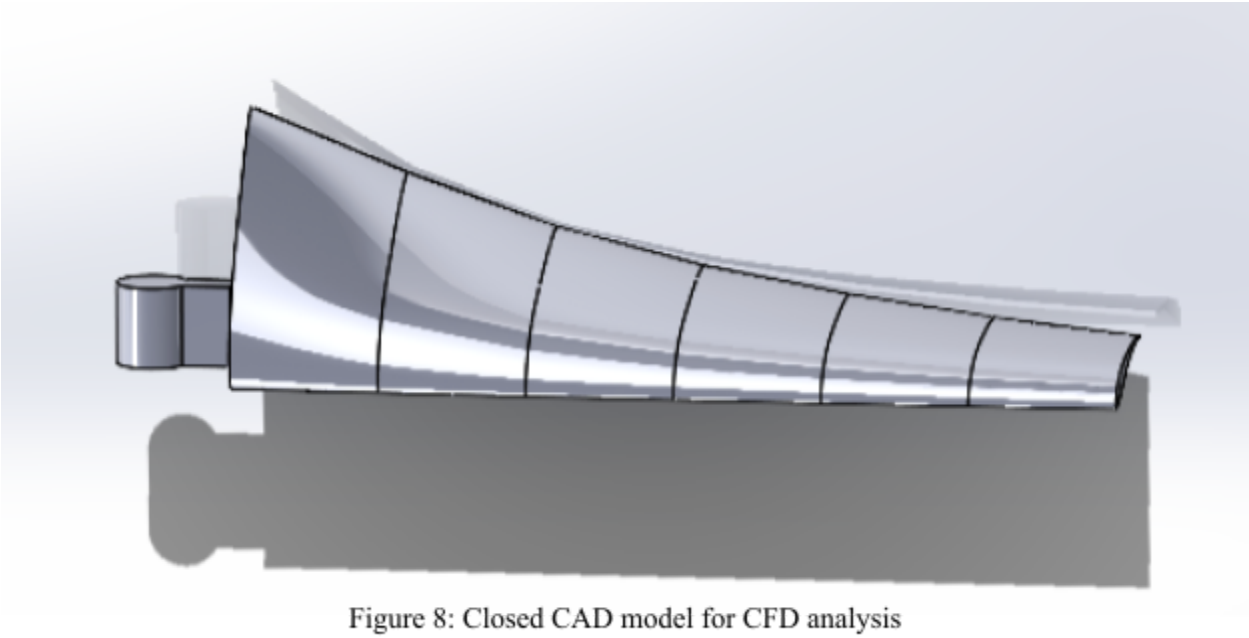

Figure 8: Closed CAD model for CFD analysis

**ANSYS Fluent Simulation:**

After finalizing our initial blade design in SolidWorks, we began working on setting up a computational fluid dynamics (CFD) simulation using ANSYS Fluent software. The process for modeling our wind turbine blade as it would actually perform in the wind tunnel can be broken down into the following steps:

**Import Geometry:**

To load our blade into ANSYS, we imported the STEP file into the SpaceClaim environment. Next, we oriented our blade so that it aligned with the positive y-axis, with the positive x-axis being the direction of fluid flow.

After properly orienting the blade, we needed to construct the fluid domain, or the region of space where the fluid would interact with the blade. This step is important because we not only wanted to model the perpendicular fluid flow over our blade, but also the flow behavior caused by the angular rotation of the blade around its axis of rotation (x-axis). To do this, we constructed a 120° wedge fully encapsulating the blade. Then we extruded it in both directions to allow for the flow to develop before it encounters the blade and also for the wake to. We didn't create a full 360° disk because we decided to utilize ANSYS Fluent's periodic boundary conditions (explained in the next step) to model its movement. Lastly, we named the surfaces that would define the boundaries of our simulation (inlet, outlet, blade wall, etc.).

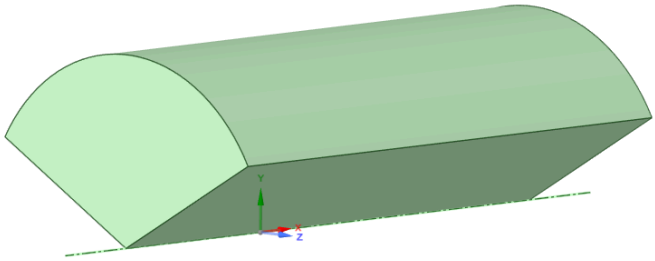

Figure 9: Fluid Domain Geometry

**Mesh Generation:**

The next step after importing the geometry was to generate the mesh. There are two types of mesh that we needed to create: the surface mesh and the volume mesh. The surface mesh tells ANSYS where the interfaces are between the fluid and the blade. In our case, we used hexagonal mesh elements as shown here:

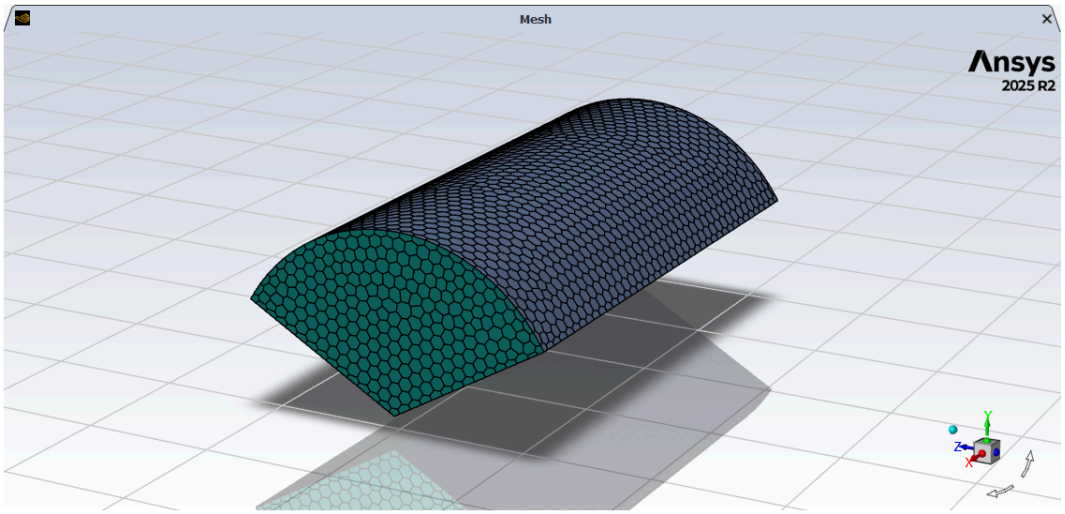


Figure 10: Fluid Domain Surface Mesh

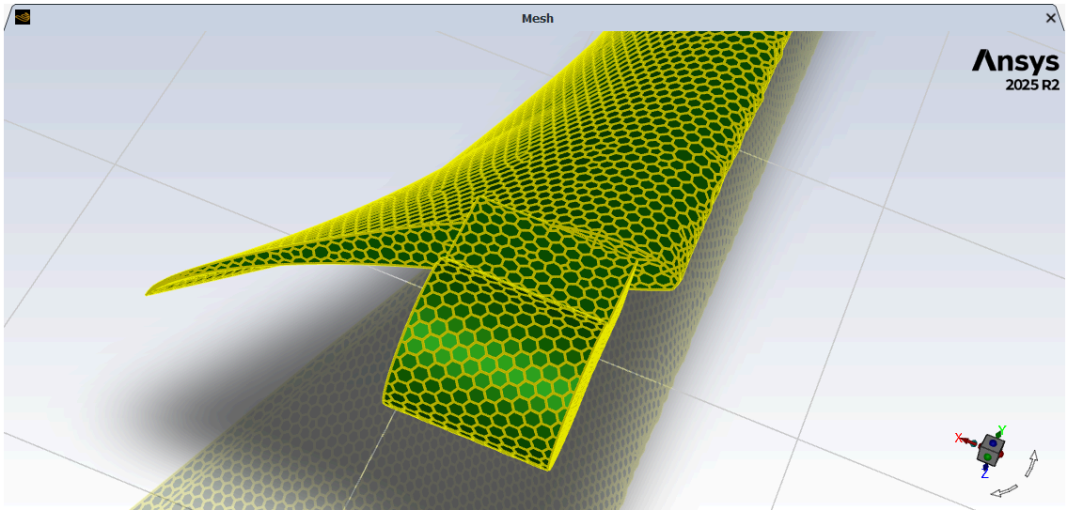


Figure 11: Blade Surface Mesh

Next, we generated the volume mesh, which uses three-dimensional polyhedral mesh elements in order to create the regions where fluid will and won't flow. When defining the mesh, we made sure to make it fine enough (minimum mesh element size) to capture the detail we needed to give us an accurate representation of the flow behavior, but not so fine as to bog down the computer leading to an unnecessarily long simulation runtime. A cross-section of the volume mesh can be seen in the image below:

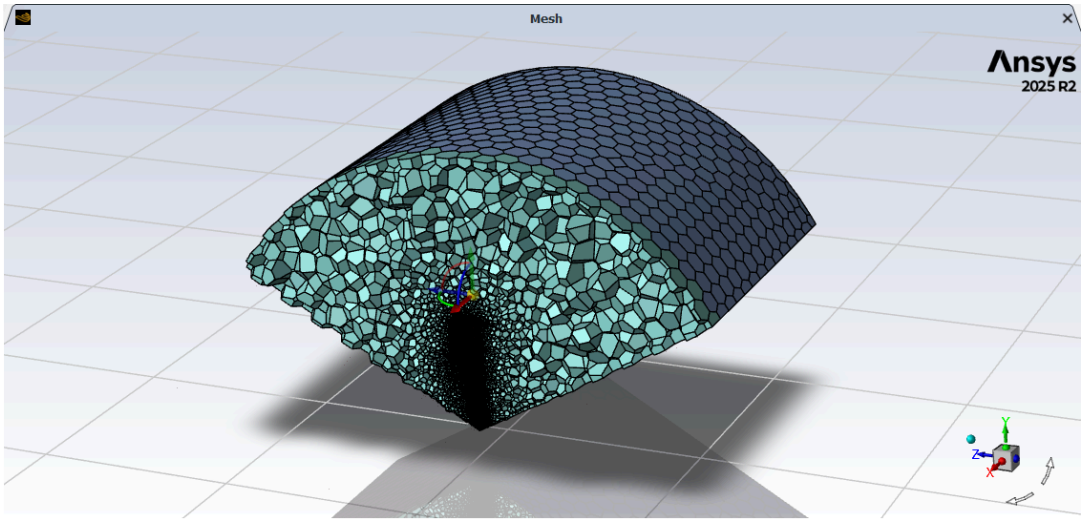


Figure 12: Volume Mesh Cross-Section

Lastly, we made use of periodic boundary conditions in ANSYS Fluent to have the fluid domain rotate around the blade (reference frame of the blade). We chose to do this to simplify the model and reduce overall simulation runtime.

**Mathematical Model Set-up:**

For the mathematical model, we chose the k-omega model as it is the most commonly used model fo simple fluid dynamics simulations such as this one. Next, we ensured that all of the simulation variables (mainly density of air = 1.2 g/cm^3 and fluid velocity = 6 m/s) were all correct.

**Numerical Solution:**

The final step before running the simulation, the solution step, we made sure to report out values for both the pressure and velocity of the fluid, as well as the torque generated by the blade about its axis of rotation. Lastly, we initialized the solution and set it to run for 1500 iterations.

**Post-Processing:**

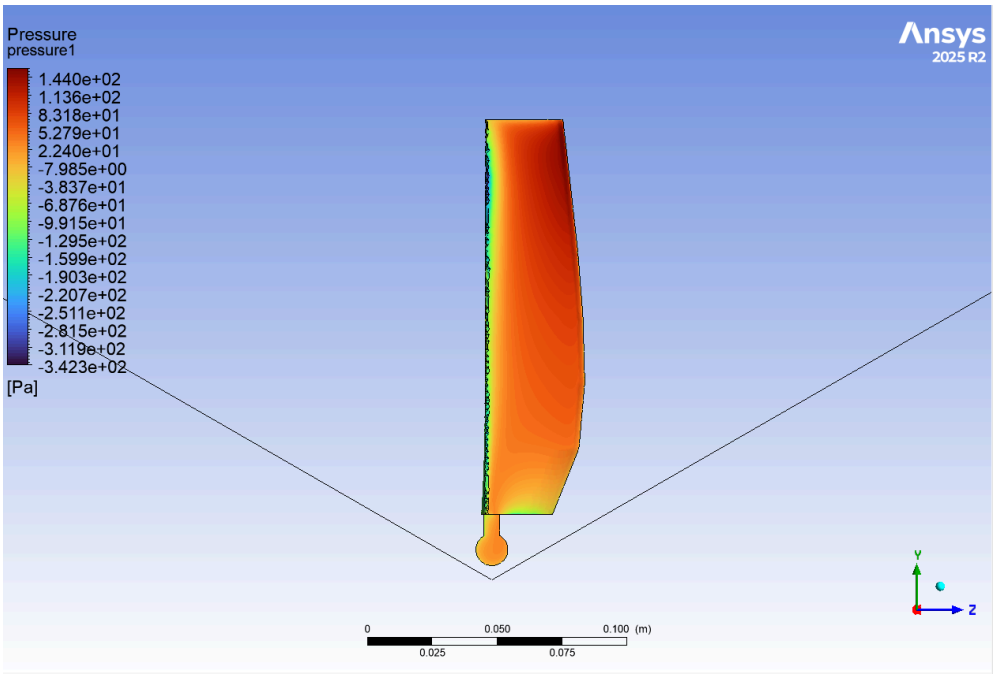


Figure 13: Pressure Contour Blade Front

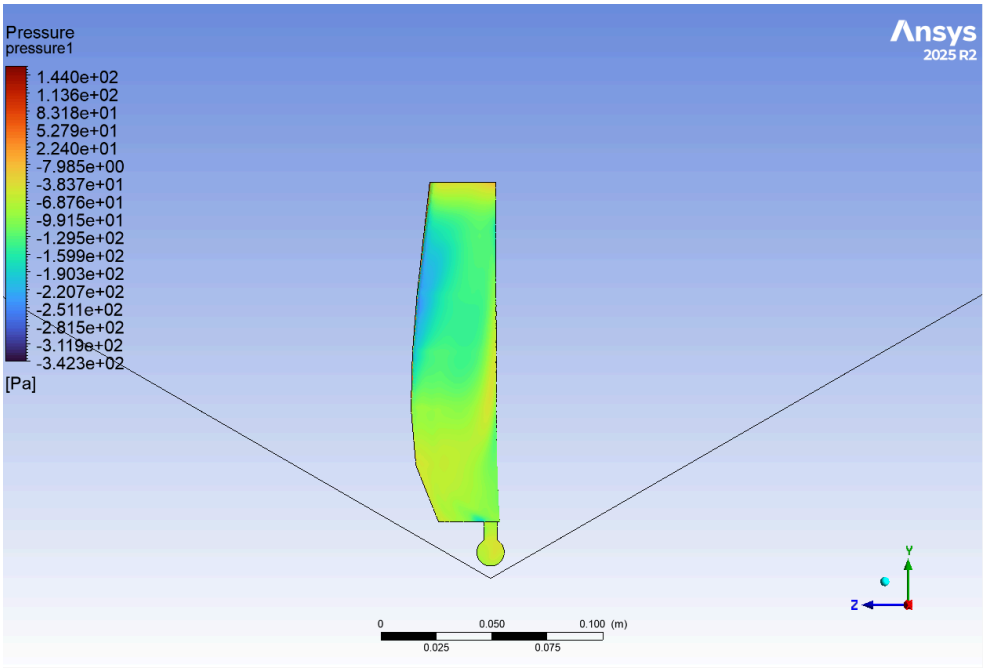


Figure 14: Pressure Contour Blade Back

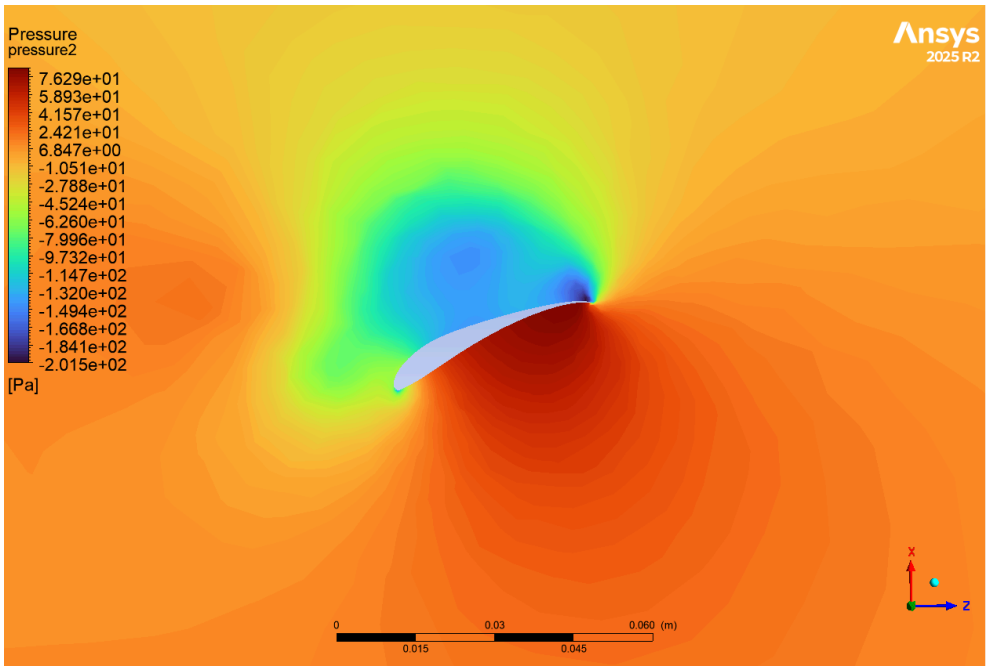


Figure 15: Pressure Contour through Blade Midspan

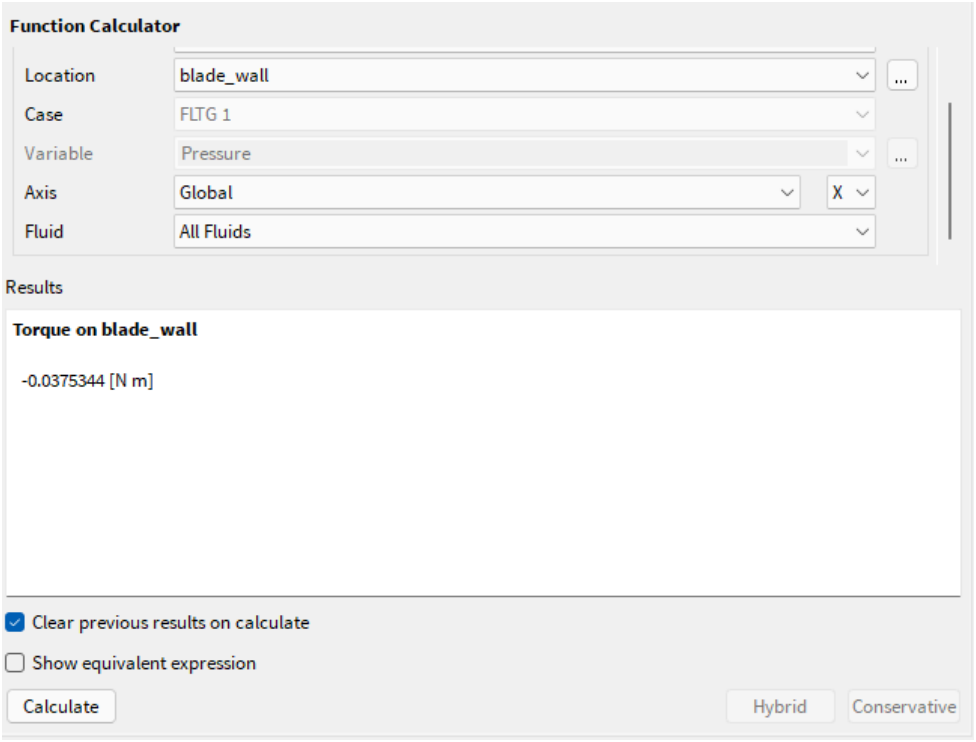


Figure 16: Torque Report

**Analysis:**

Looking at the figures above, it is expected that there will be high pressure along the front face of the blade since that is where the flow “stagnates” or is slowed down. This in turn means that there will be a region of low pressure directly behind the blade. This pressure differential on the blade is what creates a moment on it, thus causing it to generate a torque about the x-axis. Speaking of torque, the value that ANSYS calculated of -0.0375 Nm is a lower than what we were expecting because multiplying that by the fluid angular velocity of 98 rads^-1 to get the power produced by one blade, and then multiplying that number by 3, results in a total wind turbine power of approximately 11.03 W, which is considerably larger than the 3 W from our actual wind tunnel testing. We attribute this discrepancy to the k-omega model possibly not being the best model for this situation, relatively poor mesh quality, or the boundary conditions not being precise enough. These are all points that we would plan to address if we were to run this simulation again.

**CONCLUSION:**

This project successfully demonstrated a torque-optimized small-scale wind turbine blade operating in an extremely low Reynolds number regime. By prioritizing low tip-speed ratio operation, selecting the S1223 airfoil, and carefully tailoring twist and chord distributions, the design met all geometric, material, and operational constraints while achieving strong torque performance across the expected wind distribution. Experimental testing validated the core

design objective, with the blade remaining safely below brake and structural limits, and even exceeding performance expectations by achieving peak power at higher rotational speeds than initially predicted. The discrepancy between designed and measured operating speed highlights limitations in low-Re modeling assumptions and points toward clear opportunities for refinement through improved CFD meshing, more accurate induction modeling, and iteration around the 1200–1400 rpm range.

Equally important to the technical outcome was the effectiveness of our group dynamics. The team worked collaboratively across aerodynamics, structures, CAD, CFD, and testing, allowing challenges such as geometry export errors, CFD setup issues, and print imperfections to be identified and resolved efficiently. Open communication and clear task ownership helped maintain momentum when unexpected setbacks arose, particularly during the CAD-to-CFD workflow and experimental troubleshooting. This division of strengths, combined with shared problem-solving, enabled us to integrate theory, simulation, and experimentation into a cohesive final design. In a second iteration, earlier cross-checks between CAD, CFD, and manufacturing would further streamline the process, but overall, the team’s coordination and adaptability were central to the project’s success.